Oxidatively-induced μ-η^1 → μ-η^1:η^1 rearrangement of {N═N} ligands at a {Mo_2(μ-SMe)$_3$} site and protonation of the oxidized diazenido complex†

Alan Le Goff, Christine Le Roy, François Y. Pétillon, Philippe Schollhammer and Jean Talarmin*

Received (in Montpellier, France) 27th January 2006, Accepted 15th March 2006
First published as an Advance Article on the web 5th April 2006
DOI: 10.1039/b601377e

The electrochemical oxidation of [Mo_2(cp)$_2$(μ-SMe)$_3$(μ-N_2Ph)] and [Mo_2(cp)$_2$(μ-SMe)$_3$(μ-N_2HPh)]$^+$ complexes where the diazo bridge adopts either an η^1 or an η^1:η^1 coordination mode has been studied by cyclic voltammetry and controlled-potential electrolysis in THF– and CH_2Cl_2–[NBu_4][PF_6]. The electrochemical oxidation of [Mo_2(cp)$_2$(μ-SMe)$_3$(μ-η^1-N_2Ph)] **1** and of [Mo_2(cp)$_2$(μ-SMe)$_3$(μ-η^1-N_2HPh)]$^+$ **1-H**$^+$ triggers the isomerization of the diazo bridge to the η^1:η^1 mode found in **2**$^+$ and **2-H**$^{2+}$ respectively. The electrochemical oxidation of [Mo_2(cp)$_2$(μ-SMe)$_3$(μ-η^1:η^1-N_2Ph)] **3** and of [Mo_2(cp)$_2$(μ-SMe)$_3$(μ-η^1:η^1-HN_2Ph)]$^+$ **3-H**$^+$ with a *syn* ("up–up") arrangement of the Me substituents of the equatorial sulfur bridges is also followed by an isomerization to **2**$^+$ and **2-H**$^{2+}$, respectively, with an *anti* ("up–down") configuration of the equatorial Me groups. The rates of the isomerization **1**$^+$ → **2**$^+$, **1-H**$^{2+}$ → **2-H**$^{2+}$, and **3-H**$^{2+}$ → **2-H**$^{2+}$ were studied by cyclic voltammetry at different scan rates and at different temperatures. The isomerization of the protonated complexes with either a hydrazido(2−) or a diazene bridge (respectively **1-H**$^{2+}$ and **3-H**$^{2+}$) is faster than that of the diazenido precursors (respectively **1**$^+$ and **3**$^+$). The diazenido complex **2**$^+$ protonates readily, affording **2-H**$^{2+}$, while **2-H**$^{3+}$ undergoes proton loss.

Introduction

Forty years after the discovery of the first transition-metal complex containing molecular nitrogen as a ligand,[1] chemical dinitrogen fixation based on successive {H^+/e} transfer steps remains a very challenging enterprise. Research in this area has shown that a transition-metal catalyst could sustain the reduction of N_2 to NH_3.[2] Low oxidation state metal centres (Mo or W) in a phosphorus environment allowed the first electrosynthesis of ammonia[3] and make the foundation of the Chatt cycle[2,4] while investigations of higher oxidation state complexes, either (η^5-C_5Me_5)MMe_3 (M = Mo or W) or Mo[$HIPTN_3N$], recently culminated with the catalytic reduction of dinitrogen to ammonia.[5]

Some years ago, we reported studies of dinuclear {[Mo_2(cp)$_2$(μ-SMe)$_3$]$^+$} complexes in relevance to different stages of chemical nitrogen fixation.[6] Although they lack the crucial N_2-binding ability as most other metal–sulfur centres,[2,7] and as the enzyme active site, the FeMo cofactor (FeMo-co),[8] when it is separated from its proteic environment,[9–13] these complexes provided chemical precedents for the stepwise cleavage of a {N═N} bond at a bimetallic sulfur core. This involves intermediates where diazenido, hydrazido(2−) (or isodiazene), diazene, imido, amido and ammine ligands are bound to the conserved {[Mo_2(cp)$_2$(μ-SMe)$_3$]$^+$} centre (Scheme 1).[6d,f] These species are dinuclear counterparts of the intermediates involved in the Chatt and the Schrock cycles[2,4,5] which describe the stepwise reduction of N_2 at single metal centres. The results obtained with the {[Mo_2(cp)$_2$(μ-SMe)$_3$]$^+$} complexes[6] suggested that all the steps of the reduction of N_2 to NH_3 could occur at a bimetallic M(μ-S)$_2$M′ site of FeMo-co, where M and M′ may be identical or different. The dinitrogen reduction cycle which we proposed on this experimental basis[6f] differs from the schemes proposed by Durrant[15] and by Blöchl[16] on the grounds of DFT calculations, notably in the coordination mode of the diazenido ligand.

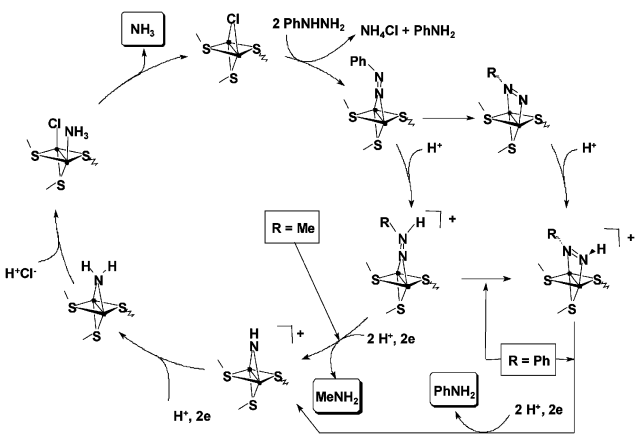

Scheme 1 ● = Mo(cp).

UMR CNRS 6521, Chimie, Electrochimie Moléculaires et Chimie Analytique, Université de Bretagne Occidentale, 6 Av. V Le Gorgeu, CS 93837, 29238 Brest Cedex 3, France. E-mail: Jean.Talarmin@univ-brest.fr

† Electronic supplementary information (ESI) available: Cyclic voltammograms and Eyring plots. See DOI: 10.1039/b601377e

However, the diazenido complexes isolated[6c] as μ-η^1 and μ-η^1:η^1 isomers are neutral (Scheme 1), while if N_2 was to bind at a $\{[Mo^{III}_2(cp)_2(\mu\text{-}SR)_3]^+\}$ core, protonation would afford a dicationic diazenido species. This prompted us to examine the oxidative electrochemistry of the $[Mo_2(cp)_2(\mu\text{-}SMe)_3(\mu\text{-}NNPh)]$ complexes. In this paper, we show that the μ-η^1 → μ-η^1:η^1 isomerism of the phenyldiazenido- and of the phenylhydrazido(2−) (or isodiazene) ligand as well as the rearrangement of a bridging thiolate in $[Mo_2(cp)_2(\mu\text{-}SMe)_3(\mu\text{-}N_2Ph)]$ and $[Mo_2(cp)_2(\mu\text{-}SMe)_3(\mu\text{-}HN_2Ph)]^+$ complexes are oxidatively-induced processes.

Structural consequences of redox steps are well documented.[17–32] Electron-transfer may bring about specific motions within a molecule that can be used to design molecular machines[20] or which modify the reactivity at a metal centre, for example *via* the exposure of a vacant coordination site,[21] including ring-slippage processes.[17,19a,22] Rearrangement of a bound substrate may also be important in regard to its activation. Examples of redox-induced reorientation of an alkyne moiety over a metal triangle, and alkyne/vinylidene interconversion are known.[23,24] In this context, redox-induced linkage isomerism has been described for a variety of ligands,[11a,25–30] η^1/η^2 coordination change of nitriles[31] or disulfide,[32] and of a carboxylate ligand.[21c] However, we are not aware of similar work concerning N═N fragments such as diazenido, hydrazido(2−) or diazene ligands, although thermal and/or photochemical conversions of this sort are known.[6c,33]

Interestingly, besides the isomerism which favours a μ-η^1:η^1 coordination mode of the NNPh and HNNPh ligands in the oxidized derivatives, this study demonstrates that the cationic diazenido complex protonates readily and also suggests that the dication is able to abstract a H atom from the environment.

Results

The synthesis, the full characterization of complexes $[Mo_2(cp)_2(\mu\text{-}SMe)_3(\mu\text{-}N_2Ph)]$ (**1**, **3**), and $[Mo_2(cp)_2(\mu\text{-}SMe)_3(\mu\text{-}N_2HPh)]^+$ (**1-H**$^+$, **3-H**$^+$) (Scheme 2), and the molecular structures of **1** and **3-H**$^+$ have been reported previously.[6c] The existence of a third isomer with a diazenido ligand, differing from **3** by the relative disposition of the methyl substituents of the equatorial sulfur bridges (**2** in Scheme 2),

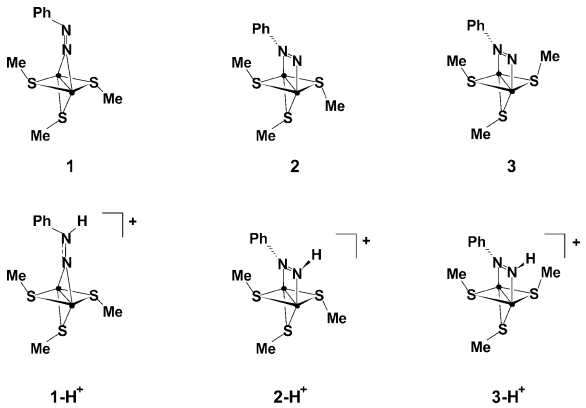

Scheme 2 ● = Mo(cp).

as well as the formation of an intermediate (**2-H**$^+$, Scheme 2) in the isomerization of **1-H**$^+$ to **3-H**$^+$ were also mentioned.[6c] The cyclic voltammograms in Fig. S1 and S2 (ESI†) are those of the starting material (**1-H**$^+$) and of the intermediate (**2-H**$^+$) formed in this reaction. The phenyldiazene complex **2-H**$^+$ in turn isomerizes to **3-H**$^+$. The electrochemical oxidation of **1**, **1-H**$^+$, **3**, and **3-H**$^+$ has been investigated in THF– and CH_2Cl_2–$[NBu_4][PF_6]$ by cyclic voltammetry and controlled-potential electrolysis. The products resulting from their oxidation can be identified by CV[34] since the first oxidation of the *syn* ("up–up") and the *anti* ("up–down") isomers of the complexes with a μ-η^1:η^1 diazenido- (**3** and **2**, respectively) or diazene bridge (**3-H**$^+$ and **2-H**$^+$, respectively) occur at different potentials (Table 1).

Oxidatively-induced μ-η^1 → μ-η^1:η^1 rearrangement of the {N═N} ligand in $[Mo_2(cp)_2(\mu\text{-}SMe)_3(\mu\text{-}\eta^1\text{-}N_2Ph)]$, 1, and $[Mo_2(cp)_2(\mu\text{-}SMe)_3(\mu\text{-}\eta^1\text{-}N_2HPh)]^+$, 1-H$^+$.

Electrochemical oxidation of $[Mo_2(cp)_2(\mu\text{-}SMe)_3(\mu\text{-}\eta^1\text{-}N_2Ph)]$, 1. Complex **1** oxidizes in two successive one-electron steps, and undergoes an irreversible reduction (E_p^{red} = −2.81 V, THF–$[NBu_4][PF_6]$)[34] (Table 1); the latter will not be discussed in this paper. The first oxidation of **1** (Scheme 3, step a) is an electrochemically reversible, diffusion-controlled one-electron process (ΔE_p = 60 mV in CH_2Cl_2, *ca.* 80 mV in THF; $i_p^{ox1}/v^{1/2}$ independent of scan rate, v), which is followed

Table 1 Redox potentials (V/Fc) of $[Mo_2(cp)_2(\mu\text{-}SMe)_3(\mu\text{-}NNPh)]$ and of $[Mo_2(cp)_2(\mu\text{-}SMe)_3(\mu\text{-}NNHPh)]^+$ complexes (CV measurements in THF– and CH_2Cl_2–$[NBu_4][PF_6]$ at v = 0.2 V s^{-1})[38b]

Compound	Solvent	E_p^{red}	$E_{1/2}^{ox1}$	E_p^{ox2}
$[Mo_2(cp)_2(\mu\text{-}SMe)_3(\mu\text{-}\eta^1\text{-}NNPh)]$, **1**	THF	−2.81	−0.30	0.39 (−20 °C)
	CH_2Cl_2	—	−0.34	0.44
anti-$[Mo_2(cp)_2(\mu\text{-}SMe)_3(\mu\text{-}\eta^1\text{:}\eta^1\text{-}NNPh)]$, **2**	THF	−2.93	−0.62	0.37 ($E_{1/2}$)[a]
	CH_2Cl_2 (18 °C)	—	−0.61	0.47 ($E_{1/2}$)[a]
	CH_2Cl_2 (−30°C)		−0.64	0.42 ($E_{1/2}$)[a]
syn-$[Mo_2(cp)_2(\mu\text{-}SMe)_3(\mu\text{-}\eta^1\text{:}\eta^1\text{-}NNPh)]$, **3**	THF	−2.93	−0.50	0.43
	CH_2Cl_2	—	−0.50	0.52
$[Mo_2(cp)_2(\mu\text{-}SMe)_3(\mu\text{-}\eta^1\text{-}NNHPh)]^+$, **1-H**$^+$	THF	−1.56[6f]	0.2 (E_p)	
	CH_2Cl_2	—	0.32	
anti-$[Mo_2(cp)_2(\mu\text{-}SMe)_3(\mu\text{-}\eta^1\text{:}\eta^1\text{-}HNNPh)]^+$, **2-H**$^+$	THF	−1.65[6f]	−0.11	0.89
	CH_2Cl_2	—	0	0.96
syn-$[Mo_2(cp)_2(\mu\text{-}SMe)_3(\mu\text{-}\eta^1\text{:}\eta^1\text{-}HNNPh)]^+$, **3-H**$^+$	THF	−1.63 ($E_{1/2}$)[6f]	0	0.89
	CH_2Cl_2	—	0.1	1.0

[a] Measured from a solution of **2**$^+$ generated by controlled-potential oxidation of **3**.

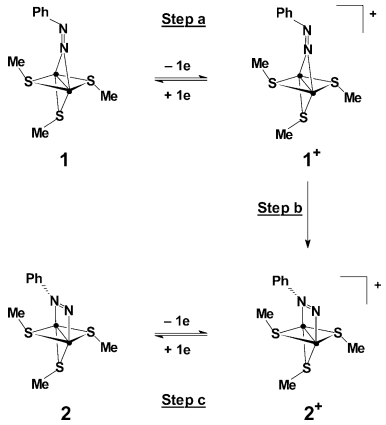

Scheme 3 ● = Mo(cp).

by a chemical reaction (Scheme 3, step b; EC process[34,35]). The reduction peak detected at $E_p^{red} = -0.65$ V on the reverse scan (Fig. 1a) is part of the reversible couple of *anti*-$[Mo_2(cp)_2(\mu\text{-}SMe)_3(\mu\text{-}\eta^1{:}\eta^1\text{-}N_2Ph)]^+$, $\mathbf{2}^+$ ($E_{1/2} = -0.62$ V, Scheme 3, step c, Fig. 1b; Table 1) produced by the oxidatively-induced isomerization. The effect of the follow-up chemical reaction is limited on increasing the scan rate or on lowering the temperature, as shown by the suppression of the product peak under these conditions (Fig. 1c). The rate constant of the μ-η¹ → μ-η¹:η¹ isomerism at the N=N–Ph bridge in the cation was obtained at different temperatures (Table 2) from measurements of the peak current ratio $[(i_p^c/i_p^a)^{ox1}]$ at different scan rates, using literature methods.[36] The activation parameters for the isomerization were derived from the linear Eyring plot $\ln(k/T) = f(1/T)$ (Fig. S3, ESI†). The temperature dependence of the rate constant and thus the activation enthalpy and entropy are different in THF and in CH_2Cl_2. This suggests a different solvation of the transition states involved in the isomerization in these solvents.

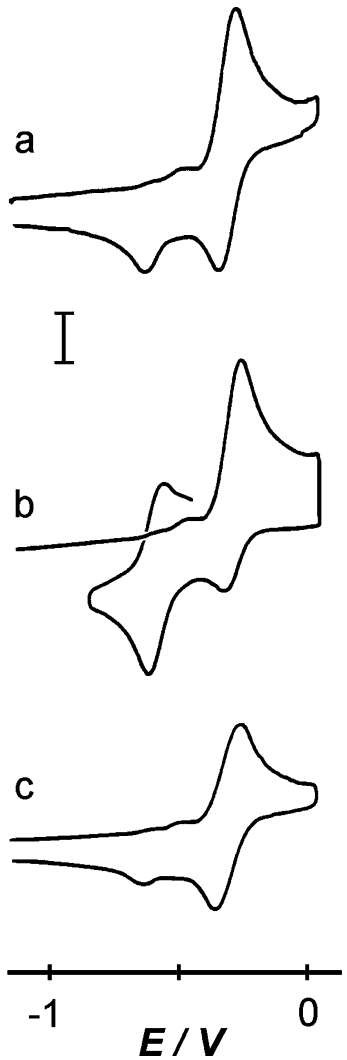

Fig. 1 Cyclic voltammetry of $[Mo_2(cp)_2(\mu\text{-}SMe)_3(\mu\text{-}\eta^1\text{-}N_2Ph)]$, **1** (0.75 mM) in THF–$[NBu_4][PF_6]$ (a) at a scan rate $v = 0.2$ V s^{-1} at 18 °C, (b) the same as in (a) with a 15 s hold at *ca.* 0.1 V, and (c) the same as in (a) at a scan rate $v = 0.5$ V s^{-1}. The current scale is 4 μA for (a) and (b) and 10 μA for (c).

Table 2 Rate constants for the μ-η¹ → μ-η¹:η¹ isomerization of the diazo bridge and for the *syn* → *anti* isomerization at a SMe group in $[Mo_2(cp)_2(\mu\text{-}SMe)_3(\mu\text{-}N_2Ph)]$ and $[Mo_2(cp)_2(\mu\text{-}SMe)_3(\mu\text{-}N_2HPh)]^+$ complexes

Reaction	Solvent	T (K)	k (s^{-1})
$\mathbf{1}^+ \rightarrow \mathbf{2}^+$	THF	261.7	0.01
		277	0.05
		291	0.25
		299	0.47
$\mathbf{1}^+ \rightarrow \mathbf{2}^+$	CH_2Cl_2	268	0.03
		275.5	0.06
		279	0.08
		289.5	0.19
$\mathbf{1\text{-}H}^{2+} \rightarrow \mathbf{2\text{-}H}^{2+}$	CH_2Cl_2	262.3	0.08
		270	0.17
		279	0.40
$\mathbf{3\text{-}H}^{2+} \rightarrow \mathbf{2\text{-}H}^{2+}$	THF	256.5	0.02
		273	0.07
		287	0.22
		308	1.21

The second oxidation in the CV of **1** at 18 °C and $v = 0.2$ V s^{-1} arises from both $\mathbf{1}^+$ and $\mathbf{2}^+$ produced by the first oxidation. This is followed by a reaction generating the diazene complex *anti*-$[Mo_2(cp)_2(\mu\text{-}SMe)_3(\mu\text{-}\eta^1{:}\eta^1\text{-}HN_2Ph)]^{2+}$, $\mathbf{2\text{-}H}^{2+}$, as evidenced by the presence of all three redox processes of this compound in the CV of **1** (Fig. S4, ESI†), indicating that the diazenido dication $\mathbf{2}^{2+}$ is able to abstract a hydrogen atom from the solvent–$[NBu_4][PF_6]$ electrolyte.

As expected from the CV experiments, controlled-potential electrolysis conducted at −0.15 V (room temperature, Pt anode, *ca.* 0.9 F mol^{-1} **1**) quantitatively[37] converts **1** to $\mathbf{2}^+$ while the solution turns from red to green–yellow. The μ-η¹ isomer **1** is not regenerated upon reduction of $\mathbf{2}^+$ (see below and Scheme 3, step c), so that the μ-η¹ → μ-η¹:η¹ rearrangement is an irreversible process under the present conditions.

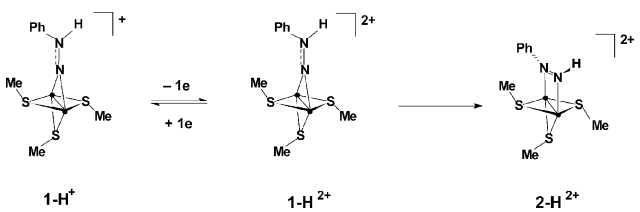

Scheme 4 ● = Mo(cp).

Table 3 Activation parameters for the μ-η^1 → μ-η^1:η^1 isomerization of the diazo bridge and for the *syn* → *anti* isomerization at a SMe group in $[Mo_2(cp)_2(\mu\text{-}SMe)_3(\mu\text{-}N_2Ph)]$ and $[Mo_2(cp)_2(\mu\text{-}SMe)_3(\mu\text{-}N_2HPh)]^+$ complexes

Reaction	Solvent	$\Delta H^{\neq}$ (kJ mol^{-1})	$\Delta S^{\neq}$ (J mol^{-1} K^{-1})	$\Delta G^{\neq}_{293}$ (kJ mol^{-1})	k_{293} (s^{-1})
$\mathbf{1}^+ \rightarrow \mathbf{2}^+$	THF	66 ± 2	−30 ± 8	74.8	0.28
$\mathbf{1}^+ \rightarrow \mathbf{2}^+$	CH_2Cl_2	53 ± 1	−75 ± 2	75.1	0.25
$\mathbf{1\text{-}H}^{2+} \rightarrow \mathbf{2\text{-}H}^{2+}$	CH_2Cl_2	56 ± 1	−50 ± 2	71.0	1.34
$\mathbf{3\text{-}H}^{2+} \rightarrow \mathbf{2\text{-}H}^{2+}$	THF	50 ± 3	−82 ± 10	74.1	0.38

Electrochemical oxidation of $[Mo_2(cp)_2(\mu\text{-}SMe)_3(\mu\text{-}\eta^1\text{-}N_2HPh)]^+$, $\mathbf{1\text{-}H}^+$. Besides the thermal isomerization process,[6c] $\mathbf{1\text{-}H}^+$ undergoes isomerization to *anti*-$[Mo_2(cp)_2(\mu\text{-}SMe)_3(\mu\text{-}\eta^1\text{:}\eta^1\text{-}HN_2Ph)]^{2+}$ $\mathbf{2\text{-}H}^{2+}$ upon electrochemical one-electron oxidation. At room temperature in THF–$[NBu_4][PF_6]$, the first irreversible ($v \leq 1$ V s^{-1}) oxidation of $\mathbf{1\text{-}H}^+$ produces $\mathbf{2\text{-}H}^{2+}$ (Scheme 4) characterized by its reversible redox couple at $E_{1/2} = -0.11$ V (Fig. S1, ESI†).

Similar observations are made in CH_2Cl_2–$[NBu_4][PF_6]$, although some reversibility of the oxidation of $\mathbf{1\text{-}H}^+$ becomes evident at scan rates larger than 0.5 V s^{-1} or at low temperature. The rate constant of the isomerization process was calculated in CH_2Cl_2–$[NBu_4][PF_6]$ from measurements of $[(i_p^c/i_p^a)^{ox}]$ at different temperatures and different scan rates[36] (Tables 2 and 3).

Oxidatively-induced inversion at a SMe group in *syn*-$[Mo_2(cp)_2(\mu\text{-}SMe)_3(\mu\text{-}\eta^1\text{:}\eta^1\text{-}N_2Ph)]$, **3**, and *syn*-$[Mo_2(cp)_2(\mu\text{-}SMe)_3(\mu\text{-}\eta^1\text{:}\eta^1\text{-}HN_2Ph)]^+$, $\mathbf{3\text{-}H}^+$.

Electrochemical oxidation of *syn*-$[Mo_2(cp)_2(\mu\text{-}SMe)_3(\mu\text{-}\eta^1\text{:}\eta^1\text{-}N_2Ph)]$, 3. Complex **3** undergoes two one-electron oxidation steps in THF– and CH_2Cl_2–$[NBu_4][PF_6]$ (Table 1) and an irreversible reduction that can be detected only in THF. The first oxidation of **3** (Scheme 5, step a) is a reversible, diffusion-controlled step followed by a slow chemical reaction which is not detectable by CV $[(i_p^c/i_p^a)^{ox1} \sim 1$, Fig. 2a], but is observed on the longer time scale of electrolysis (Scheme 5, step b). Thus, controlled-potential oxidation of **3** produced $\mathbf{2}^+$ essentially quantitatively[37] after *ca.* 0.9 F mol^{-1} **3** had been consumed. The first reduction of $\mathbf{2}^+$ (Scheme 5, step c) is a diffusion-controlled, reversible one-electron step on the CV time scale at room temperature [ΔE_p = 70–80 mV in THF– and CH_2Cl_2–$[NBu_4][PF_6]$; $(i_p^a/i_p^c)^{red} = 0.87$ at $v = 0.02$ V s^{-1}; 1.0 at $v = 0.1$ V s^{-1} in THF]. As could be anticipated from the lower value of the peak current ratio $[(i_p^a/i_p^c)^{red}]$ at slow scan rate, controlled-potential reduction of $\mathbf{2}^+$ at −1.0 V (room temperature, Pt cathode) yields a mixture of **2** and **3**, the isomerization of **2** to **3** being slow (Scheme 5, step d); the ratio **3**/**2** increases when the catholyte is allowed to stand under Ar.

In some systems the isomerization step is accelerated by, or arises only after, the transfer of two electrons. In the present case, the second oxidation of **3** (Scheme 5, step e) is coupled to different chemical reactions. Isomerism at a SMe bridge is evidenced by the detection of the reduction of $\mathbf{2}^+$ on the reverse scan (Fig. 2b, peak C; Scheme 5, steps f and g). The formation of protonated species is again demonstrated by the presence of reduction peaks around 0 V (Fig. 2b, peak A) and −1.6 V (not shown in Fig. 2b). The rounded shape of peak A (Fig. 2b) suggests that the *syn* ($\mathbf{3\text{-}H}^{2+}$) and *anti* ($\mathbf{2\text{-}H}^{2+}$) isomers of the diazene complex are both present (Scheme 5, steps h and i). The oxidation of $\mathbf{3}^+$ also affords an unidentified product with a reversible couple (Fig. 2b, peak B) observed at different potentials in THF and CH_2Cl_2 (−0.31 V and −0.15 V, respectively). The formation of both the protonated species and of the unknown product is suppressed at low temperature (Fig. 3b).

Although the oxidation of *syn*-$[Mo_2(cp)_2(\mu\text{-}SMe)_3(\mu\text{-}\eta^1\text{:}\eta^1\text{-}N_2Ph)]^+$, $\mathbf{3}^+$, looks reversible at low temperature (*ca.* −45 °C, CH_2Cl_2 electrolyte), isomerization has occurred since the product detected on the reverse scan at the potential of the first redox step is the *anti* isomer $\mathbf{2}^+$ (Fig. 3b).[38] Low temperature CV shows an abrupt current rise from the onset of the second oxidation peak in the CV of **3** (Fig. 3b, T = −46 °C, CH_2Cl_2–$[NBu_4][PF_6]$); scan reversal immediately after the

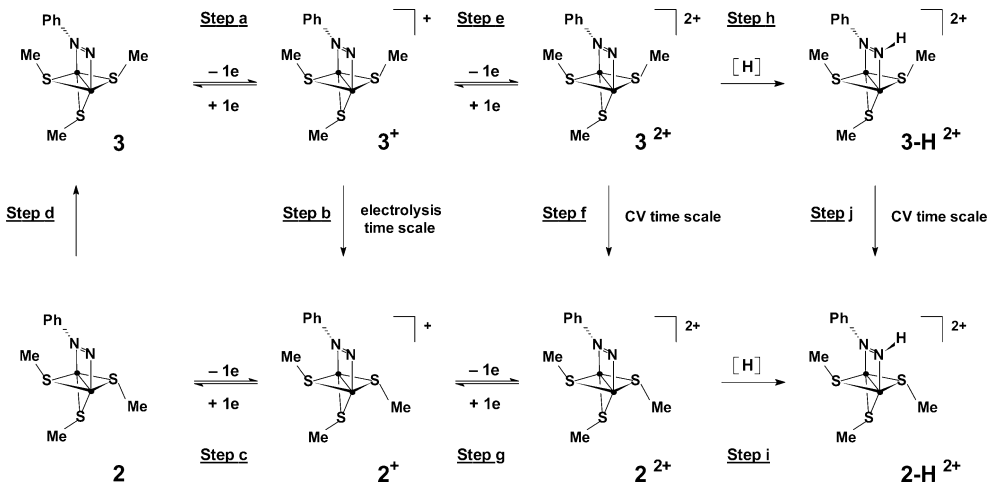

Scheme 5 ● = Mo(cp); the reaction(s) leading to the unidentified product (see text) is (are) not indicated; step j is discussed below.

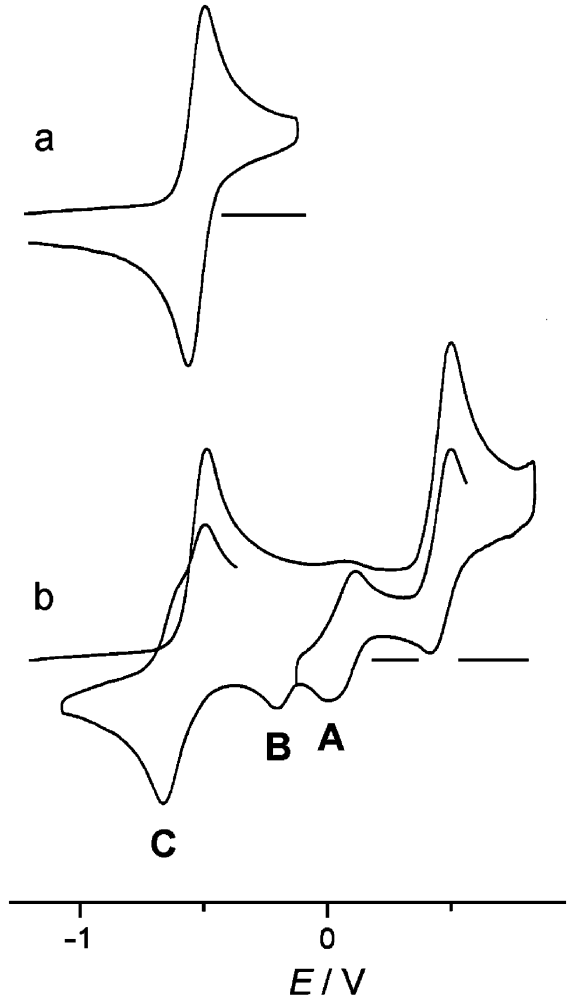

Fig. 2 Cyclic voltammetry of *syn*-$[Mo_2(cp)_2(\mu\text{-}SMe)_3(\mu\text{-}\eta^1{:}\eta^1\text{-}N_2Ph)]$, **3** in CH_2Cl_2–$[NBu_4][PF_6]$ at 18 °C. In (a) the scan is limited to the first, reversible, oxidation of **3**, and in (b) it includes the second oxidation process, giving rise to $\mathbf{2}^+$ (peak C), to protonated species (peak A) and to an unidentified product (peak B) (see text) (v = 0.2 V s^{-1}; vitreous carbon electrode).

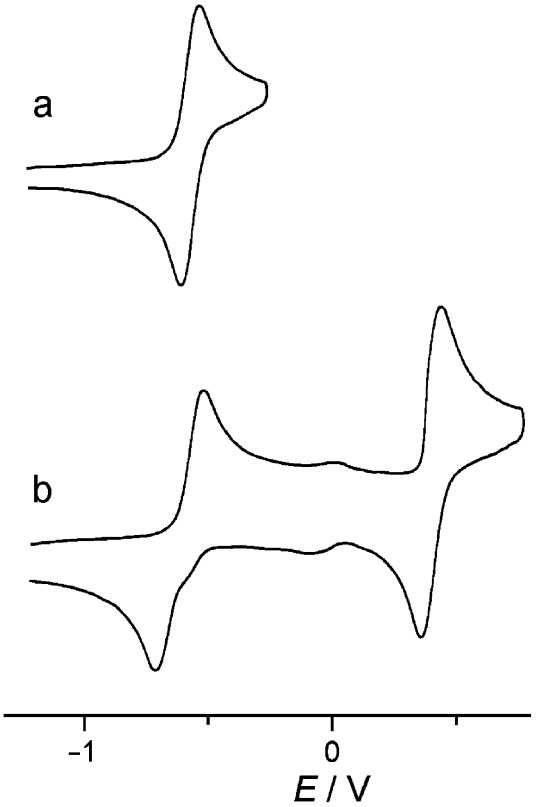

Fig. 3 Cyclic voltammetry of *syn*-$[Mo_2(cp)_2(\mu\text{-}SMe)_3(\mu\text{-}\eta^1{:}\eta^1\text{-}N_2Ph)]$, **3**, in CH_2Cl_2–$[NBu_4][PF_6]$ at −46 °C; the difference between scans (a) and (b) is only the potential range (v = 0.2 V s^{-1}; vitreous carbon electrode).

associated reduction peak has been traversed leads to the detection of a reversible couple at a potential slightly less positive than the oxidation peak of $\mathbf{3}^+$ on the initial positive scan (Fig. S5, ESI†). This indicates that $\mathbf{2}^+$ oxidizes at a slightly less positive potential than $\mathbf{3}^+$ under these conditions. The fast isomerization of $\mathbf{3}^{2+}$ to $\mathbf{2}^{2+}$ would drive a cross redox reaction producing $\mathbf{2}^+$ from $\mathbf{3}^+$. The abrupt rise of the current is assigned to the fact that $\mathbf{2}^+$ resulting from the homogeneous reaction is generated at a potential positive of the $\mathbf{2}^+/\mathbf{2}^{2+}$ transition and is thus immediately oxidized.

Electrochemical oxidation of *syn*-$[Mo_2(cp)_2(\mu\text{-}SMe)_3(\mu\text{-}\eta^1{:}\eta^1\text{-}HN_2Ph)]^+$, $\mathbf{3\text{-}H}^+$. Complexes (*syn*) $\mathbf{3\text{-}H}^+$ and (*anti*) $\mathbf{2\text{-}H}^+$ undergo two oxidation steps (Table 1). The first one is an electrochemically reversible, diffusion-controlled one-electron process (Scheme 6, step a), whereas the second is irreversible. The first oxidation of $\mathbf{3\text{-}H}^+$ is followed by isomerization to $\mathbf{2\text{-}H}^{2+}$ (Scheme 6, step b), which is suppressed on lowering the temperature (Fig. 4a, T = −45 °C, CH_2Cl_2 electrolyte; similar CVs are obtained in THF) or on increasing the scan rate. The rate constant for the isomerization was calculated from measurements of the peak current ratio $[(i_p^c/i_p^a)^{ox1}]$ at different scan rates[36] and at different temperatures (Table 2); the activation parameters were derived from the linear Eyring plot (R^2 = 0.994) (Table 3).

The oxidation of $\mathbf{3\text{-}H}^{2+}$ is an irreversible process, and the follow-up chemical reactions are still observed by CV at low temperature in CH_2Cl_2– (Fig. 4b), and in THF–$[NBu_4][PF_6]$. Dissociation of the proton from the diazo bridge of the undetected $\mathbf{3\text{-}H}^{3+}$ (Scheme 7, step a) would be consistent with the presence of a small peak around 0.4 V on the reverse scan

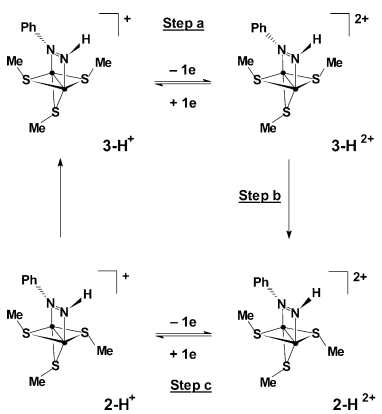

Scheme 6 ● = Mo(cp).

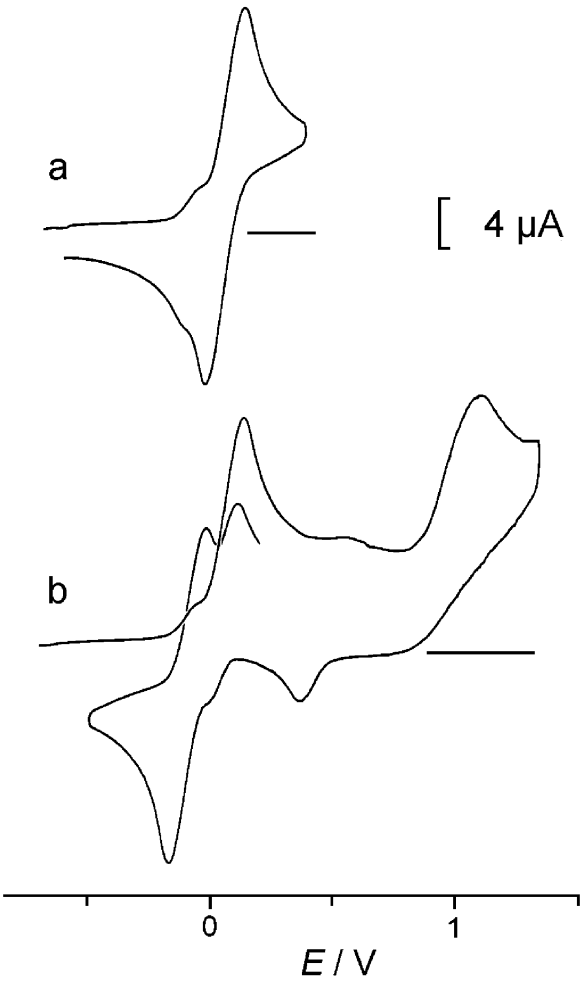

Fig. 4 Cyclic voltammetry of $[Mo_2(cp)_2(\mu\text{-}SMe)_3(\mu\text{-}\eta^1{:}\eta^1\text{-}HN_2Ph)]^+$ (present essentially as **3-H**$^+$) (1 mM) in CH_2Cl_2–$[NBu_4][PF_6]$ at −45 °C; in (a) the potential range is limited to the reversible oxidation of **3-H**$^+$, while in (b) it is extended to the second oxidation step that results in *syn*/*anti* isomerization (vitreous carbon electrode, $v = 0.2$ V s^{-1}).

(Fig. 4b) that is at the same potential as the reduction of $\mathbf{2}^{2+}$. The reduction around 0.4 V produces $\mathbf{2}^+$ which reacts with H^+ to afford **2-H**$^{2+}$ (Scheme 7, steps b and c). The occurrence of the latter reaction has been checked in a separate experiment by addition of HBF_4–Et_2O at −45 °C to an electrogenerated solution of $\mathbf{2}^+$ in CH_2Cl_2–$[NBu_4][PF_6]$. This results in an instant colour change from green–yellow to red–orange and in the replacement of the redox processes of $\mathbf{2}^+$ by those of **2-H**$^{2+}$ (Fig. 5b).[39]

In this case, the net *syn* → *anti* isomerization of **3-H**$^{2+}$ (Scheme 7) involves the diazenido derivative(s) *via* a deprotonation–protonation sequence.

Discussion

The isomerization steps

The μ-η^1 → μ-η^1:η^1 isomerism. The above results show that the favoured mode of coordination of the diazo moiety in the oxidized complexes is the μ-η^1:η^1 mode. Thus, the rearrangement of the diazenido ligand which occurs slowly for the neutral complex[6c] is accelerated by a one-electron oxidation of $[Mo_2(cp)_2(\mu\text{-}SMe)_3(\mu\text{-}\eta^1\text{-}N_2Ph)]$, **1**, the **1** → $\mathbf{2}^+$ conversion being detectable on the CV time scale. It was previously noted[6f] that the thermal isomerism at the diazo bridge is facilitated when the {N═N} moiety is protonated, although the migration of a proton is required in addition to the μ-η^1 → μ-η^1:η^1 coordination change. This is also true for the oxidatively-induced process, since the $[Mo_2(cp)_2(\mu\text{-}SMe)_3(\mu\text{-}\eta^1\text{-}N_2HPh)]^{2+}$ → $[Mo_2(cp)_2(\mu\text{-}SMe)_3(\mu\text{-}\eta^1{:}\eta^1\text{-}HN_2Ph)]^{2+}$ reaction is faster than $\mathbf{1}^+$ → $\mathbf{2}^+$ (Table 3). The activation parameters derived from the kinetic measurements in CH_2Cl_2 show that the energy barrier for the μ-η^1 → μ-η^1:η^1 rearrangement is lower for the diazenido ligand than for the hydrazido(2−) (or isodiazene) by *ca.* 3 kJ mol^{-1}; nevertheless, the former reaction is slower due to a more unfavourable activation entropy (Table 3) which suggests a more ordered transition state in the case of the diazenido complex compared to the hydrazido(2−) (or isodiazene) one.

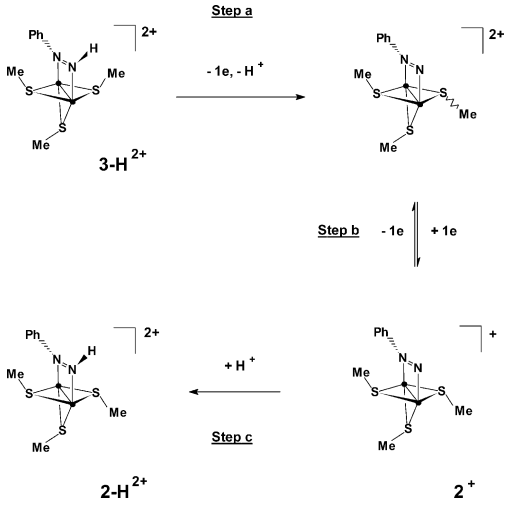

Scheme 7 ● = Mo(cp).

The reasons why the μ-η^1 → μ-η^1:η^1 isomerization of the diazenido complex is favoured upon oxidation are not clear. Although approximate theoretical methods cannot address the question of how the redox events affect the structure and the charge distribution of a complex,[40a] EHMO calculations provide information on the nature of the redox orbitals that may lead to a qualitative understanding of the origins of the structure changes.[17f,22a,40b,41–43] Calculations at the EH level on the redox orbitals of **3-H**$^+$ [6f] were consistent with later results obtained at a more sophisticated level of theory (DFT).[44] EHMO calculations carried out on simplified models of **1** and **2**, where the substituent of the {NN} ligand was replaced by H (respectively **1′** and **2′**), show that the HOMO (highest occupied molecular orbital) which is involved in the oxidation of $[Mo_2(cp)_2(\mu\text{-}SMe)_3(\mu\text{-}\eta^1\text{-}N_2H)]$, **1′**, is a metal-based [92% δ*(Mo–Mo)] orbital with no contribution from the diazenido ligand (Fig. 6a). The HOMO of *anti*-$[Mo_2(cp)_2(\mu\text{-}SMe)_3(\mu\text{-}\eta^1{:}\eta^1\text{-}N_2H)]$, **2′**, is essentially a metal–metal non-bonding δ-type orbital (Mo1 d_{xy}: 34%; Mo2 d_{xy}: 44%, see Fig. 6b; Mo2 is the N(H) bonded metal centre), with a contribution from the lone pairs of the bridging sulfur

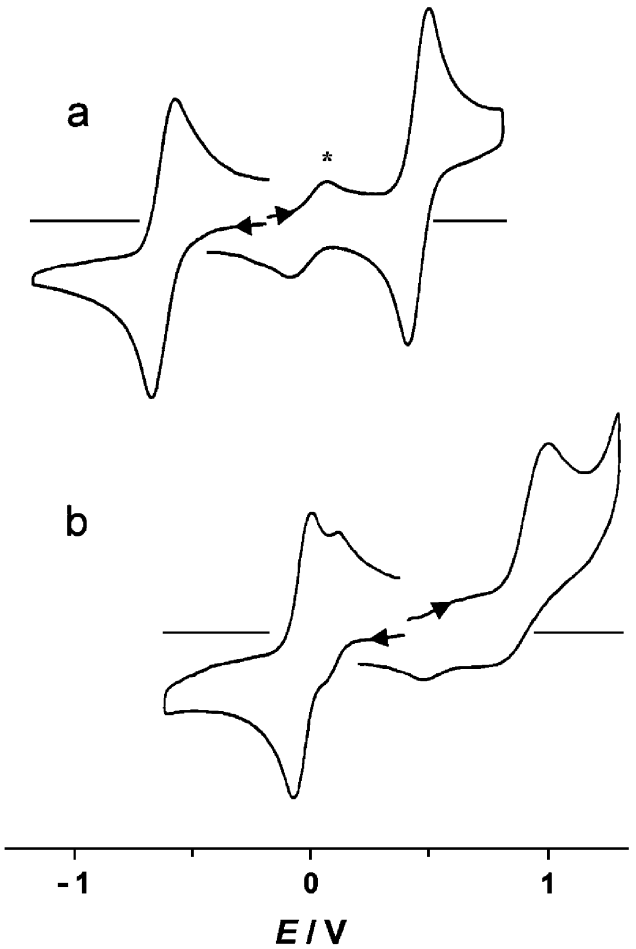

Fig. 5 Cyclic voltammetry of a CH_2Cl_2–$[NBu_4][PF_6]$ solution of *anti*-$[Mo_2(cp)_2(\mu\text{-}SMe)_3(\mu\text{-}\eta^1{:}\eta^1\text{-}N_2Ph)]^+$, $\mathbf{2}^+$ generated by controlled-potential oxidation of **3** (a) before and (b) after addition of HBF_4–Et_2O. Curve (b) shows the formation of the diazene complex *anti*-$[Mo_2(cp)_2(\mu\text{-}SMe)_3(\mu\text{-}\eta^1{:}\eta^1\text{-}HN_2Ph)]^{2+}$ $\mathbf{2\text{-}H}^{2+}$ (T = −30 °C; v = 0.2 V s^{-1}; vitreous carbon electrode).

atoms (<10% overall) and a minor contribution from the {N═N} fragment. A comparison of the orbital interaction diagrams of the $\{[Mo_2(cp)_2(\mu\text{-}SMe)_3]^+\}$ core with the {N═N} ligand in the $\mu\text{-}\eta^1$ and $\mu\text{-}\eta^1{:}\eta^1$ modes suggests a reason why the latter might be preferred since it allows a transfer of electrons from the metal centres to the ligand *via* a bonding interaction between the filled δ* and the empty N═N π* orbital, which is absent in **1′**. The antibonding counterpart of this interaction forms the LUMO (lowest unoccupied molecular orbital) of **2′**.

The *syn* → *anti* isomerism. Complexes with the $\{[Mo_2(cp)_2(\mu\text{-}SR)_n]\}$ (n = 2 or 3) core display *syn* ("up–up") or *anti* ("up–down") arrangements of the R substituents of the (equatorial when n = 3) μ-S atoms.[6,45] In contrast to the **3**, **2** and $\mathbf{3\text{-}H}^+$, $\mathbf{2\text{-}H}^+$ couples of isomers, their redox potentials are probably too close to be distinguished in most cases. However, *syn* and *anti* isomers of complexes with the $[Mo_2(cp)_2(\mu\text{-}SR)_2]$ core and a Mo═Mo double bond (R = Me, i-Pr, Ph, CF_3) can be differentiated by their redox potentials.[45b] The factors that govern the differences or similarities in the redox potentials of couples of *syn*/*anti* isomers are not known.

Although the *syn* disposition of the Me substituents appears to be thermodynamically favoured with respect to the *anti* conformation in the $\mu\text{-}\eta^1{:}\eta^1$ neutral diazenido and cationic diazene complexes, both can coexist.[46] In contrast, the most stable species at the singly oxidized level present the *anti* arrangement of the equatorial Me substituents ($\mathbf{2}^+$ and $\mathbf{2\text{-}H}^{2+}$). The isomerism at a SMe group is still favoured by a further oxidation of the complex: whereas the *syn* → *anti* isomerization of the $\mu\text{-}\eta^1{:}\eta^1$-diazenido cation is slow (CPE time scale[34]), it is much faster for the dications since the $\mathbf{3}^{2+}$ → $\mathbf{2}^{2+}$ conversion is observed by CV, even at low temperature (Fig. 3b). Like the $\mu\text{-}\eta^1$ → $\mu\text{-}\eta^1{:}\eta^1$ coordination change, isomerism at the SMe bridge is also faster for the protonated complex $\mathbf{3\text{-}H}^{2+}$ than for $\mathbf{3}^+$, as shown by the fact that it is detected on the CV time scale for $\mathbf{3\text{-}H}^{2+}$ while observable only on the longer time scale of CPE for $\mathbf{3}^+$.

Activation parameters derived from NMR data have been reported for sulfur inversion in various thiolate-bridged dinuclear complexes. The values of the free energy of activation for *syn* ↔ *anti* isomerism reported for dimolybdenum and diruthenium complexes[47] are lower by 3 to 21 kJ mol^{-1} than those computed for the (*syn*) $\mathbf{3\text{-}H}^{2+}$ → (*anti*) $\mathbf{2\text{-}H}^{2+}$ reaction at the same temperatures as the published $\Delta G^{\neq}$. The difference in the free energy of activation would be even larger if one considered the neutral diazenido and the cationic diazene complexes. This is

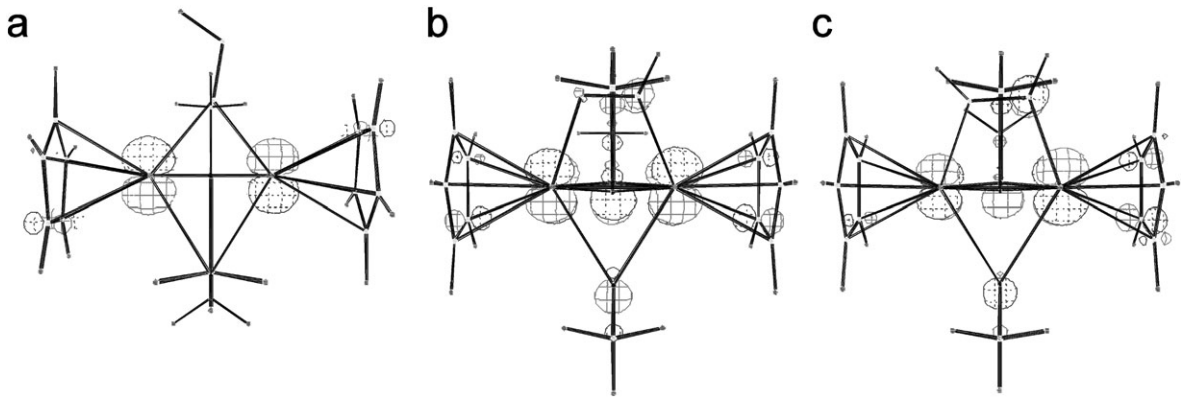

Fig. 6 A representation of the HOMO of simplified models (substituent of the {NN} ligand replaced by H) of (a) **1**, (b) **3** and (c) $\mathbf{3\text{-}H}^+$. The HOMO of **2′** is almost the same as that of **3′** shown in (b); the z axis corresponds to the Mo–Mo vector.

consistent with the facts that the *syn* (**3** and **3-H**$^+$) to *anti* (**2** and **2-H**$^+$) conversion is slow and that both isomers are observable by ^{1}H NMR spectroscopy at room temperature.

Reactivity of the oxidized complexes towards proton and hydrogen atoms

The diazenido cation *anti*-$[Mo_2(cp)_2(\mu\text{-}SMe)_3(\mu\text{-}\eta^1\text{:}\eta^1\text{-}N_2Ph)]^+$ **2**$^+$ generated by controlled-potential oxidation of *anti*-$[Mo_2(cp)_2(\mu\text{-}SMe)_3(\mu\text{-}\eta^1\text{-}N_2Ph)]$ **1** or *syn*-$[Mo_2(cp)_2(\mu\text{-}SMe)_3(\mu\text{-}\eta^1\text{:}\eta^1\text{-}N_2Ph)]$ **3** undergoes reversible one-electron reduction and oxidation steps at low temperature (Fig. 5a). However, at room temperature the oxidation is followed by chemical reactions, one of them affording **2-H**$^{2+}$ *via* the reaction of **2**$^{2+}$ with a source of hydrogen atoms. Controlled-potential oxidations of **2**$^+$ or **3** at 0.5 V effectively produce **2-H**$^{2+}$, unambiguously characterized by its three redox potentials (Table 1), along with unidentified products. The characteristic redox processes of **2-H**$^{2+}$ are also detected in the cyclic voltammogram of complex **1** when the scan is extended to the positive limit of the potential window (see arrows in Fig. S4, ESI†).

While the diazene complex **2-H**$^{3+}$ deprotonates, the diazenido cation **2**$^+$ reacts with acid to afford **2-H**$^{2+}$ in a fast reaction that still takes place at low temperature (Fig. 5). From the reactions in Scheme 8 and the redox data in Table 1, the effect of the oxidation of the complexes on their pK_a can be estimated.[48] In THF, each one-electron oxidation lowers the pK_a of the diazene complex by more than 8 units [pK_a(**2-H**$^{2+}$) − pK_a(**2-H**$^{3+}$) ∼ 8.8; pK_a(**2-H**$^+$) − pK_a(**2-H**$^{2+}$) = 8.6. The corresponding figures in CH_2Cl_2 are ∼10.5 and 9.0, respectively]. The wide pK_a range covered (*ca.* 17 units in THF; 19 in CH_2Cl_2)[48] is consistent with **2** (and **3**) being rather strongly basic species while the twice oxidized diazene complexes **2-H**$^{3+}$ (and **3-H**$^{3+}$) must be fairly strong acids.

The redox-dependence of the acid–base properties of the complexes appears not to be directly related to the nature of the orbital involved in the oxidation processes. EHMO calculations on a simplified model of complex **3** (with the Ph substituent replaced by H) indicate that the HOMO, like that of **2**, is mainly a δ orbital with little {N═N} character (Fig. 6b). The HOMO of a model of **3-H**$^+$ also possesses strong metal character (Mo1 d_{xy}: 21%; Mo2 d_{xy}: 61%, Fig. 6c) with a minor contribution from the diazene ligand. This is consistent with the results of DFT calculations.[44] The stepwise oxidation of the complexes is thus a metal-centered process that changes the Mo^{III}–Mo^{III} core of **2**, **3**, **2-H**$^+$ and **3-H**$^+$ into Mo^{IV}–Mo^{IV} in **2**$^{2+}$ and **3**$^{2+}$ (**2-H**$^{3+}$ and **3-H**$^{3+}$ were not detected under our experimental conditions).

Conclusion

The present work provides, as far as we know, the first example of an oxidatively-induced μ-η^1 → μ-η^1:η^1 isomerization of bridging diazenido and hydrazido(2−) ligands. These results also lead to the following conclusions which may be of interest for the initial steps of chemical nitrogen fixation at a $\{[Mo_2(cp)_2(\mu\text{-}SR)_3]^+\}$ site.

1 The μ-η^1:η^1 coordination of the phenyldiazenido ligand at the $\{[Mo^{III}_2(cp)_2(\mu\text{-}SMe)_3]^+\}$ site is favoured by the oxidation of the complex. This suggests that a dicationic diazenido species which would result from the protonation of a dinitrogen molecule bound at $\{[Mo^{III}_2(cp)_2(\mu\text{-}SR)_3]^+\}$ would also likely display a μ-η^1:η^1 coordination of the {N═N} fragment.

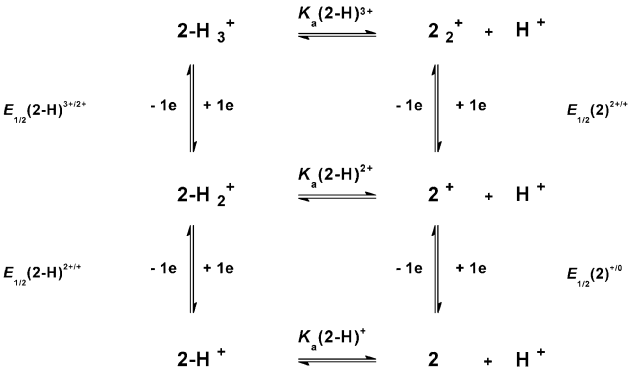

Scheme 8

2 The reduction of the phenyldiazenido dication is a metal-centered process taking place around 0.4–0.5 V (Table 1). It is likely that the reduction of an unsubstituted diazenido dication bound at the dimolybdenum core would also occur at a fairly positive potential and be metal-centered (δ orbital).

3 The redox state of the metal core modulates the acid–base properties at the {N═N} ligand. The cationic phenyldiazenido complex **2**$^+$ was shown to protonate readily. This should also be the case for an unsubstituted, cationic diazenido complex.

4 The reduction of the phenyldiazene dications **2-H**$^{2+}$ and **3-H**$^{2+}$ is a metal-centered process (δ-type orbital) which occurs in the range from −0.1 to 0.1 V. It can be anticipated that the reduction of an unsubstituted diazene analogue would also occur at a modestly negative potential.

Theoretical DFT calculations[44] have identified the essential role of the δ orbital at different stages of the electrochemical reduction of **3-H**$^+$ in acidic medium,[6f] since it serves as a source of electrons for the cleavage of the π and σ components of the N═N bond.[44]

Together with these calculations, the fact that the LUMO of the dicationic Mo^{IV}–Mo^{IV} diazenido dication is a δ orbital suggests that this orbital might also be involved in a metal → ligand electron transfer in the early steps of N_2 reduction at a Mo^{III}–Mo^{III} site derived from $\{[Mo_2(cp)_2(\mu\text{-}SMe)_3]^+\}$. Work is in progress in our group to investigate that possibility.

Experimental

Methods and materials

All the experiments were carried out under an inert atmosphere, using Schlenk techniques for the syntheses. Tetrahydrofuran (THF) and dichloromethane were purified as described previously.[6] Fluoroboric acid [diethyl ether complex (Aldrich)] was used as received. The complexes $[Mo_2(cp)_2(\mu\text{-}SMe)_3(\mu\text{-}NNPh)]$ (**1**, **3**) and $[Mo_2(cp)_2(\mu\text{-}SMe)_3(\mu\text{-}NNHPh)]^+$ (**1-H**$^+$–**3-H**$^+$) were prepared according to reported procedures.[6c]

The preparation and the purification of the $[NBu_4][PF_6]$ supporting electrolyte were as described previously.[6e] The electrochemical equipment comprised of a GCU potentiostat (Tacussel/Radiometer) driven by a PAR 175 Universal Programmer; CV traces were recorded with a SEFRAM TGM

164 X-Y recorder, and coulometric charges were obtained using an IG5-N integrator (Tacussel/Radiometer). The cell and electrodes were as described previously.[6e] All the potentials (text, tables, figures) are quoted against the ferrocene–ferrocenium couple; ferrocene was added as an internal standard at the end of the experiments.

Kinetic experiments

The kinetic data were derived from cyclic voltammetric experiments in a thermostated cell, by measurements of the peak current ratio (i_p^c/i_p^a) of the oxidation processes at different scan rates according to reported methods.[36b] The different values of the scan rate were selected so as to maintain the values of the peak current ratio between *ca.* 0.4 and 0.85. The corresponding values of $\log(k\tau)$ (where τ is the time needed to scan from $E_{1/2}$ to the switching potential) were worked out from the published data.[36a] The temperature was controlled using Huber HS 40 equipment.

EH calculations

Extended Hückel calculations were performed with the CACAO package developed by Mealli and Proserpio.[49] Standard atomic parameters were taken for H, C, and N.[50] The exponents (ζ) and the valence shell ionization potential (H_{ii} in eV) used for Mo are the standard CACAO parameters,[49] that is, respectively, 1.956 and −8.34 for 5s and 1.921 and −5.24 for 5p. The H_{ii} value for 4d was −10.50; a linear combination of two Slater-type orbitals ($\zeta_1 = 4.54$, $c_1 = 0.5899$; $\zeta_2 = 1.900$, $c_2 = 0.5899$) was used to represent the atomic 4d orbitals.

The models used in the calculations for **1** and **3-H**$^+$ were built from the crystallographically determined bond lengths and bond angles of these complexes,[6c] (except C–H = 1.09 Å and N–H = 1.01 Å) with the Ph ring replaced by H. **3′** (model of **3**) was derived from the dimensions of $[Mo_2(cp)_2(\mu\text{-}SMe)_3(\mu\text{-}\eta^1{:}\eta^1\text{-}NNMe)]$,[6g] where the methyl substituent of the diazenido ligand was replaced by an H atom. **2′** was derived from **3′** by the inversion at an equatorial S atom.

Acknowledgements

The authors thank the CNRS (Centre National de la Recherche Scientifique) and UBO (Université de Bretagne Occidentale) for financial support.

References

1 A. D. Allen and C. V. Senoff, *Chem. Commun.*, 1965, 621.
2 (*a*) F. Barrière, M. C. Durrant and C. J. Pickett, in *Catalysts for Nitrogen Fixation Nitrogenases, Relevant Chemical Models and Commercial Processes*, ed. B. E. Smith, R. L. Richards and W. E. Newton, Kluwer Academic Publishers, The Netherlands, 2004, ch. 7, pp. 161–199; (*b*) D. J. Evans, R. A. Henderson and B. E. Smith, in *Bioinorganic Catalysis*, ed. J. Reejdik and E. Bouwman, Marcel Dekker, New York, 2nd edn, 1999, ch. 7, pp. 153–207; (*c*) B. A. McKay and M. D. Fryzuk, *Chem. Rev.*, 2004, **104**, 385; (*d*) F. Barrière, *Coord. Chem. Rev.*, 2003, **236**, 71; (*e*) D. Sellmann and J. Sutter, *JBIC, J. Biol. Inorg. Chem.*, 1996, **1**, 587; (*f*) D. Coucouvanis, *JBIC, J. Biol. Inorg. Chem.*, 1996, **1**, 594; (*g*) M. Hidai and Y. Mizobe, *Chem. Rev.*, 1995, **95**, 1115 and references cited therein.
3 (*a*) C. J. Pickett and J. Talarmin, *Nature*, 1985, **317**, 652; (*b*) C. J. Pickett, K. S. Ryder and J. Talarmin, *J. Chem. Soc., Dalton Trans.*, 1986, 1453.
4 C. J. Pickett, *JBIC, J. Biol. Inorg. Chem.*, 1996, **1**, 601.
5 For reduction of N_2 at the $[HIPTN_3N]Mo$ site, see: (*a*) D. V. Yandulov and R. R. Schrock, *Science*, 2003, **301**, 76; (*b*) R. R. Schrock, *Chem. Commun.*, 2003, 2389; (*c*) R R Schrock, *Acc. Chem. Res.*, 2005, **38**, 955 and references therein. For the energetics of the Schrock cycle, also see: ; (*d*) F. Studt and F. Tuczek, *Angew. Chem., Int. Ed.*, 2005, **44**, 5639. For reduction of N_2 at the $\{Cp^*Me_3M\}$ site, see: ; (*e*) R. R. Schrock, T. E. Glassman, M. G. Vale and M. Kol, *J. Am. Chem. Soc.*, 1993, **115**, 1760; (*f*) M. G. Vale and R. R. Schrock, *Inorg. Chem.*, 1993, **32**, 2767; (*g*) T. E. Glassman, M. G. Vale and R. R. Schrock, *J. Am. Chem. Soc.*, 1992, **114**, 8098; (*h*) T. E. Glassman, M. G. Vale and R. R. Schrock, *Inorg. Chem.*, 1992, **31**, 1985; (*i*) T. E. Glassman, A. H. Liu and R. R. Schrock, *Inorg. Chem.*, 1991, **30**, 4723; (*j*) R. R. Schrock, T. E. Glassman and M. G. Vale, *J. Am. Chem. Soc.*, 1991, **113**, 725; (*k*) T. E. Glassman, M. G. Vale and R. R. Schrock, *Organometallics*, 1991, **10**, 4046; (*l*) R. R. Schrock, R. M. Kolodziej, A. H. Liu, W. M. Davis and M. G. Vale, *J. Am. Chem. Soc.*, 1991, **110**, 4338; (*m*) M. B. O'Regan, A. H. Liu, W. C. Finch, R. R. Schrock and W. M. Davis, *J. Am. Chem. Soc.*, 1990, **112**, 4331; (*n*) R. C. Murray and R. R. Schrock, *J. Am. Chem. Soc.*, 1985, **107**, 4557.
6 (*a*) P. Schollhammer, F. Y. Pétillon, S. Poder-Guillou, J.-Y. Saillard, J. Talarmin and K. W. Muir, *Chem. Commun.*, 1996, 2633; (*b*) F. Y. Pétillon, P. Schollhammer and J. Talarmin, *J. Chem. Soc., Dalton Trans.*, 1997, 4019; (*c*) P. Schollhammer, E. Guénin, F. Y. Pétillon, J. Talarmin, K. W. Muir and D. S. Yufit, *Organometallics*, 1998, **17**, 1922; (*d*) F. Y. Pétillon, P. Schollhammer, J. Talarmin and K. W. Muir, *Inorg. Chem.*, 1999, **38**, 1954; (*e*) J.-Y. Cabon, C. Le Roy, K. W. Muir, F. Y. Pétillon, F. Quentel, P. Schollhammer and J. Talarmin, *Chem.–Eur. J.*, 2000, **6**, 3033; (*f*) N. Le Grand, K. W. Muir, F. Y. Pétillon, C. J. Pickett, P. Schollhammer and J. Talarmin, *Chem.–Eur. J.*, 2002, **8**, 3115; (*g*) P. Schollhammer, B. Didier, N. Le Grand, F. Y. Pétillon, J. Talarmin, K. W. Muir and S. J. Teat, *Eur. J. Inorg. Chem.*, 2002, 658.
7 (*a*) D. Sellmann, B. Hautsch, A. Rösler and F. W. Heinemann, *Angew. Chem., Int. Ed.*, 2001, **40**, 1505 and references cited therein; (*b*) D. Sellmann, B. Hautsch, A. Rösler and F. W. Heinemann, *Angew. Chem.*, 2001, **113**, 1553.
8 (*a*) J. Kim and D. C. Rees, *Science*, 1992, **257**, 1677; (*b*) J. Kim and D. C. Rees, *Science*, 1993, **260**, 792; (*c*) S. M. Mayer, B. M. Lawson, C. A. Gormal, M. Roe and B. E. Smith, *J. Mol. Biol.*, 1999, **292**, 871; (*d*) O. Einsle, F. A. Tezcan, S. L. Andrade, B. Schmid, M. Yoshida, J. B. Howard and D. C. Rees, *Science*, 2002, **297**, 1696.
9 B. E. Smith, M. C. Durrant, S. A. Fairhurst, C. A. Gormal, K. L. C. Grönberg, R. A. Henderson, S. K. Ibrahim, T. Le Gall and C. J. Pickett, *Coord. Chem. Rev.*, 1999, **185–186**, 669 and references cited therein.
10 F. A. Schultz, S. F. Gheller, B. K. Burgess, S. Lough and W. E. Newton, *J. Am. Chem. Soc.*, 1985, **107**, 5364.
11 (*a*) C. J. Pickett, K. A. Vincent, S. K. Ibrahim, C. A. Gormal, B. E. Smith and S. P. Best, *Chem.–Eur. J.*, 2003, **9**, 76; (*b*) C. J. Pickett, K. A. Vincent, S. K. Ibrahim, C. A. Gormal, B. E. Smith, S. A. Fairhurst and S. P. Best, *Chem.–Eur. J.*, 2004, **10**, 4770.
12 K. L. C. Grönberg, C. A. Gormal, M. C. Durrant, B. E. Smith and R. A. Henderson, *J. Am. Chem. Soc.*, 1998, **120**, 10613.
13 Dinitrogen has been reported to competitively inhibit the catalytic reduction of acetylene by isolated FeMo-co reduced by Eu/Hg,[14] which indicates that N_2 binds to the isolated cofactor; however, electrochemical studies of NMF solutions of isolated FeMo-co revealed no difference in the cyclic voltammograms obtained under Ar or under N_2, even at pressures up to 12 atm N_2[11a].
14 M. A. Bazhenova, T. A. Bazhenova, G. N. Petrova and S. A. Mironova, *Kinet. Catal.*, 2002, **43**, 592.
15 M. C. Durrant, *Biochemistry*, 2002, **41**, 13934.
16 J. Kästner and P. E. Blöchl, *ChemPhysChem*, 2005, **6**, 1724.
17 Structural consequences of electron-transfer reactions have been thoroughly investigated by W. E. Geiger and co-workers in a series of articles; for leading references, see: (*a*) W. E. Geiger, *Acc. Chem. Res.*, 1995, **28**, 351; (*b*) W. E. Geiger, *Prog. Inorg. Chem.*, 1985, **33**, 275 and references therein; (*c*) M. P. Robben, P. H. Rieger and W. E. Geiger, Structural Consequences of Electron-Transfer Reactions, Part 35, *J. Am. Chem. Soc.*, 1999, **121**, 367; (*d*) A. Garg, D. M. Nemer, H. Choi, J. B. Sheridan and W. E. Geiger, *Organometallics*, 2006, **25**, 275; (*e*) M. J. Shaw, J. Hyde,

C. White and W. E. Geiger, *Organometallics*, 2004, **23**, 2205; (*f*) M. E. Stoll, P. Belanzoni, M. J. Calhorda, M. G. B. Drew, V. Felix, W. E. Geiger, C. A. Gamelas, I. S. Gonçalves, C. C. Romão and L. F. Veiros, *J. Am. Chem. Soc.*, 2001, **123**, 10595 and references cited therein.

18 D. H. Evans, K. M. O'Connell, *Electroanalytical Chemistry*, ed. A. J. Bard, Marcel Dekker, New York, 1986, vol. 14, p. 113.

19 (*a*) C. Amatore, A. Ceccon, S. Santi and J.-N. Verpeaux, *Chem.–Eur. J.*, 1999, **5**, 3357; (*b*) M. F. C. Guedes da Silva, J. J. R. Frausto da Silva, A. J. L. Pombeiro, C. Amatore and J.-N. Verpeaux, *Inorg. Chem.*, 1998, **37**, 2344 and references cited therein.

20 (*a*) L. Fabbrizzi and A. Poggi, *Chem. Soc. Rev.*, 1995, 197; (*b*) L. Fabbrizzi, M. Licchelli and P. Pallavicini, *Acc. Chem. Res.*, 1999, **32**, 846; (*c*) P. R. Ashton, R. Ballardini, V. Balzani, S. E. Boyd, A. Credi, M. T. Gandolfi, M. Gomez-Lopez, S. Iqbal, D. Philp, J. A. Preece, L. Prodi, H. G. Ricketts, J. F. Stoddart, M. S. Tolley, M. Venturi, A. J. P. White and D. J. Williams, *Chem.–Eur. J.*, 1997, **3**, 152; (*d*) V. Balzani, M. Gomez-Lopez and J. F. Stoddart, *Acc. Chem. Res.*, 1998, **31**, 405; (*e*) J.-P. Sauvage, *Acc. Chem. Res.*, 1998, **31**, 611 and references therein.

21 (*a*) A. M. Allgeier and C. A. Mirkin, *Angew. Chem., Int. Ed.*, 1998, **37**, 894 and references therein; (*b*) F. Barrière, Y. Le Mest, F. Y. Pétillon, S. Poder-Guillou, P. Schollhammer and J. Talarmin, *J. Chem. Soc., Dalton Trans.*, 1996, 3967; (*c*) D. L. Hughes, S. K. Ibrahim, C. J. Pickett, G. Querné, A. Laouénan, J. Talarmin, A. Queiros and A. Fonseca, *Polyhedron*, 1994, **13**, 3341.

22 (*a*) W. E. Geiger, P. H. Rieger, C. Corbato, J. Edwin, E. Fonseca, G. A. Lane and J. M. Mevs, *J. Am. Chem. Soc.*, 1993, **115**, 2314; (*b*) C. A. Gamelas, E. Herdtweck, J. P. Lopes and C. C. Romao, *Organometallics*, 1999, **18**, 506.

23 (*a*) D. Osella, L. Pospisil and J. Fiedler, *Organometallics*, 1993, **12**, 3140; (*b*) R. Rumin, F. Robin-Le Guen, J. Talarmin and F. Y. Pétillon, *Organometallics*, 1994, **13**, 1155.

24 N. G. Connelly, W. E. Geiger, M. C. Lagunas, B. Metz, A. L. Rieger, P. H. Rieger and M. J. Shaw, *J. Am. Chem. Soc.*, 1995, **117**, 12202.

25 (*a*) A. Yeh, N. Scott and H. Taube, *Inorg. Chem.*, 1982, **21**, 2542; (*b*) W. D. Harman, M. Sekine and H. Taube, *J. Am. Chem. Soc.*, 1988, **110**, 2439; (*c*) W. D. Harman and H. Taube, *J. Am. Chem. Soc.*, 1988, **110**, 5403; (*d*) D. P. Fairlie, Y. Ilan and H. Taube, *Inorg. Chem.*, 1997, **36**, 1029.

26 D. W. Powell and P. A. Lay, *Inorg. Chem.*, 1992, **31**, 3542.

27 D. O. Silva and H. Toma, *Can. J. Chem.*, 1994, **72**, 1705.

28 A. O. Tomita and M. Sano, *Inorg. Chem.*, 1994, **33**, 5825.

29 D. Ooyama, N. Nagao, H. Nagao, Y. Miura, A. Hasegawa, K. Ando, F. S. Howell, M. Mukaida and K. Tanaka, *Inorg. Chem.*, 1995, **34**, 6024.

30 (*a*) W. E. Geiger, N. C. Ohrenberg, B. Yeomans, N. G. Connelly and D. J. H. Emslie, *J. Am. Chem. Soc.*, 2003, **125**, 8680; (*b*) N. G. Connelly, D. J. H. Emslie, W. E. Geiger, O. D. Hayward, E. B. Linehan, A. G. Orpen, M. J. Quayle and P. H. Rieger, *J. Chem. Soc., Dalton Trans.*, 2001, 670; (*c*) N. G. Connelly, D. J. H. Emslie, B. Metz, A. G. Orpen and M. J. Quayle, *Chem. Commun.*, 1996, 2289.

31 D. Lucas, Z. Modarres-Tehrani, Y. Mugnier, A. Antinolo, I. Del Hierro, A. Otero and M. Fajardo, *New J. Chem.*, 1996, **20**, 385.

32 (*a*) K. Yoshioka, H. Kikuchi, J. Mizutani and K. Matsumoto, *Inorg. Chem.*, 2001, **40**, 2234; (*b*) S. Inomata, H. Tobita and H. Ogino, *Inorg. Chem.*, 1991, **30**, 3039; (*c*) H. Brunner, A. Merz, J. Pfauntsch, O. Serhadli, J. Wachter and M. L. Ziegler, *Inorg. Chem.*, 1988, **27**, 2055.

33 (*a*) D. Sutton, *Chem. Rev.*, 1993, **93**, 995 and references therein; (*b*) D. E. Samkoff, J. R. Shapley, M. Rowen Churchill and H. J. Wasserman, *Inorg. Chem.*, 1984, **23**, 397.

34 The parameters i_p and E_p are respectively the peak current and the peak potential of a redox process; $E_{1/2} = (E_p^a + E_p^c)/2$; $\Delta E_p = E_p^a - E_p^c$; E_p^a, i_p^a and E_p^c, i_p^c are respectively the potential and the current of the anodic and of the cathodic peak of a reversible process; an EC process comprises an electron transfer step (E) followed by a chemical reaction (C). CV and CPE stand for cyclic voltammetry and controlled-potential electrolysis, respectively.

35 (*a*) A. J. Bard and L. R. Faulkner, *Electrochemical Methods Fundamentals and Applications*, Wiley, New York, 1980, ch. 11, pp. 429–485; (*b*) E. R. Brown and R. F. Large, in *Techniques of Chemistry, Volume I – Physical Methods of Chemistry*, Part IIA, ed. A. Weissberger, Wiley, 1971, ch. 6, pp. 423–530.

36 (*a*) R. S. Nicholson and I. Shain, *Anal. Chem.*, 1964, **36**, 706; (*b*) R. S. Nicholson, *Anal. Chem.*, 1966, **38**, 1406.

37 The yield was obtained by CV, by comparison of the peak current of the product(s) of the controlled-potential electrolysis to that of the one-electron oxidation of the starting material, assuming identical diffusion coefficients.

38 (*a*) This shows that $\mathbf{3}^{2+} \rightarrow \mathbf{2}^{2+}$ is a fast reaction even at low temperature, so that the return peak observed around 0.31 V (THF) or 0.44 V (CH_2Cl_2) in the CV of **3** at room temperature (Fig. 2b) is likely due to the reduction of $\mathbf{2}^{2+}$; (*b*) consequently, the oxidation potential of $\mathbf{3}^{+}$ given in Table 1 is the peak potential (E_p^{ox2}). For isomer **2**, the value of $E_{1/2}^{ox2}$ in Table 1 was measured from solutions of $\mathbf{2}^{+}$ generated by controlled-potential electrolysis.

39 The protonation of $\mathbf{2}^{+}$ to $\mathbf{2\text{-}H}^{2+}$ also suggests that the minor reversible couple detected around 0 V before addition of acid (Fig. 5a) may result from the formation of a small amount of $\mathbf{X\text{-}H}^{2+}$ by reaction of $\mathbf{X}^{+}$ (X = **2** and **3**) with an unidentified proton source. Reduction of $\mathbf{X\text{-}H}^{2+}$ either electrochemically (E_{appl} = −0.2 V) or chemically (by the starting material **3**) during the electrolysis would afford $\mathbf{X\text{-}H}^{+}$. The CV recorded after addition of acid (Fig. 5b) shows that both $\mathbf{2\text{-}H}^{2+}$ (major reduction couple) and $\mathbf{3\text{-}H}^{2+}$ (minor couple) are present. The latter cannot arise from the addition of acid to the electrolyzed solution since the only diazenido cation detected at this stage is $\mathbf{2}^{+}$. The *reduction* of $\mathbf{3\text{-}H}^{2+}$ is observed in Fig. 5b because the start potential of the scan is positive to the $E_{1/2}$ of the $\mathbf{3\text{-}H}^{2+}/\mathbf{3\text{-}H}^{+}$ couple, so that this isomer present in solution as $\mathbf{3\text{-}H}^{+}$ is oxidized in the diffusion layer, prior to the start of the potential scan. This is confirmed by the detection of a small *oxidation* current at the start potential when the solution is stirred.

40 (*a*) M.-H. Baik, T. Ziegler and C. K. Schauer, *J. Am. Chem. Soc.*, 2000, **122**, 9143; (*b*) Y. Koide, M. T. Bautista, P. S. White and C. K. Schauer, *Inorg. Chem.*, 1992, **31**, 3690.

41 D. Urhammer and F. A. Schultz, *J. Phys. Chem. A*, 2002, **106**, 11630.

42 (*a*) A. Morneau, W. E. Geiger, M. G. Richmond, M.-J. Don, W. H. Watson and A. Nagl, *Organometallics*, 2002, **21**, 1247; (*b*) T. A. Albright, W. E. Geiger, J. Moraczewski and B. Tulyathan, *J. Am. Chem. Soc.*, 1981, **103**, 4787.

43 (*a*) J.-F. Capon, R. Kergoat, N. Le Berre-Cosquer, S. Péron, J.-Y. Saillard and J. Talarmin, *Organometallics*, 1997, **16**, 4645; (*b*) M. El Khalifa, J.-Y. Saillard, F. Gloaguen, C. Le Floch, F. Y. Pétillon and J. Talarmin, *New J. Chem.*, 1992, **16**, 847; (*c*) M. El Khalifa, F. Y. Pétillon, J.-Y. Saillard and J. Talarmin, *Inorg. Chem.*, 1989, **28**, 3849.

44 J. K. Padden Metzker and J. E. McGrady, *Chem.–Eur. J.*, 2004, **10**, 6447.

45 (*a*) F. Y. Pétillon, P. Schollhammer, J. Talarmin and K. W. Muir, *Coord. Chem. Rev.*, 1998, **178–180**, 203; (*b*) M.-L. Abasq, D. L. Hughes, F. Y. Pétillon, R. Pichon, C. J. Pickett and J. Talarmin, *J. Chem. Soc., Dalton Trans.*, 1997, 2279.

46 This is observed after controlled-potential reduction of $\mathbf{2}^{+}$ that leads to a mixture of **2** and **3**. Also, samples of $\mathbf{3\text{-}H}^{+}$ contain small amounts of $\mathbf{2\text{-}H}^{+}$, as can be seen in Fig. 4.

47 (*a*) M. L. H. Green and D. K. P. Ng, *J. Chem. Soc., Dalton Trans.*, 1993, 11; (*b*) Q. Feng, M. Ferrer, M. L. H. Green, P. Mountford, V. S. B. Mtetwa and K. Prout, *J. Chem. Soc., Dalton Trans.*, 1991, 1397; (*c*) I. B. Benson, S. A. R. Knox, P. J. Naish and A. J. Welch, *J. Chem. Soc., Dalton Trans.*1981, 2235; (*d*) S. D. Killops and S. A. R. Knox, *J. Chem. Soc., Dalton Trans.*, 1978, 1260; (*e*) I. B. Benson, S. A. R. Knox, P. J. Naish and A. J. Welch, *J. Chem. Soc., Chem. Commun.*, 1978, 878.

48 The figure for $[pK_a(\mathbf{2\text{-}H}^{2+}) - pK_a(\mathbf{2\text{-}H}^{3+})]$ is only approximate due to the fact that the oxidation of $\mathbf{2\text{-}H}^{2+}$ is irreversibleunder the conditions of this study; thus, the oxidation potential for $\mathbf{2\text{-}H}^{2+/3+}$ has no thermodynamic significance. The half-wave potential $E_{1/2}$ was taken as a good approximation to $E^{\circ\prime}$ (see ref. 35*a*, ch. 5, p. 160).

49 C. Mealli and D. M. Proserpio, *J. Chem. Educ.*, 1990, **67**, 399.

50 (*a*) R. Hoffmann, *J. Chem. Phys.*, 1963, **39**, 1397; (*b*) R. Hoffmann and W. N. Lipscomb, *J. Chem. Phys.*, 1962, **36**, 2179.

